Density Functional Theory Study of the Geometry, Energetics, and Reconstruction Process of Si(111) Surfaces

Santiago D. Solares,[†] Siddharth Dasgupta,[†,‡] Peter A. Schultz,[§] Yong-Hoon Kim,[†,||] Charles B. Musgrave,[†,⊥] and William A. Goddard III*,[†]

Materials and Process Simulation Center, California Institute of Technology, Pasadena, California 91125, and Multiscale Computational Materials Methods Department, Sandia National Laboratories, Albuquerque, New Mexico 87185

Received July 26, 2005. In Final Form: September 20, 2005

We report the structures and energies from first principles density functional calculations of 12 different reconstructed (111) surfaces of silicon, including the 3 × 3 to 9 × 9 dimer−adatom−stacking fault (DAS) structures. These calculations used the Perdew−Burke−Ernzerhof generalized gradient approximation of density functional theory and Gaussian basis functions. We considered fully periodic slabs of various thicknesses. We find that the most stable surface is the DAS 7 × 7 structure, with a surface energy of 1.044 eV/1 × 1 cell (1310 dyn/cm). To analyze the origins of the stability of these systems and to predict energetics for more complex, less-ordered systems, we develop a model in which the surface energy is partitioned into contributions from seven different types of atom environments. This analysis is used to predict the surface energy of larger DAS structures (including their asymptotic behavior for very large unit cells) and to study the energetics of the sequential size change (SSC) model proposed by Shimada and Tochihara for the observed dynamical reconstruction of the Si(111) 1 × 1 structure. We obtain an energy barrier at the 2 × 2 cell size and confirm that the 7 × 7 regular stage of the SSC model (corresponding to the DAS 7 × 7 reconstruction) provides the highest energy reduction per unit cell with respect to the unreconstructed Si(111) 1 × 1 surface.

1. Introduction

One of the finest examples of experiment and theory working together to explain a very complex phenomenon is the elucidation of the atomistic structure underlying the 7 × 7 reconstruction of Si(111). After Schlier and Farnsworth[1] first observed the seventh-order spots in the low-energy electron diffraction (LEED) pattern in 1959, numerous models of this surface reconstruction were proposed on the basis of various experiments and calculations.[2−4] Most were proven wrong by the first STM experiments (1981).[5] Eventually the surface reconstruction was successfully interpreted in terms of the dimer−adatom−stacking fault (DAS) model by Takayanagi et al. (1985).[6,7] This model involves dimers, adsorbed atoms, and stacking faults and is now well validated through many theoretical and experimental studies.[8−28] Takayanagi's work was followed by a series of theoretical calculations, including ab initio cluster calculations (Northrup[22,23]), empirical and semiempirical calculations (Qian and Chadi,[24,25] Khor and Das Sarma[12]), and large-scale fully periodic ab initio calculations (Brommer et al.[16] and Stich et al.[20]), which demonstrated that the DAS model is fundamentally correct and provided a quantitative understanding of its electronic structure.

Despite the successful characterization of the DAS 7 × 7 surface, many questions remain concerning the dynamical processes involved in forming this complex structure (say from a freshly cleaved surface) and the role these processes may play in the growth and etching of various structures. Although the reconstruction process has been recently observed in real time,[8] little is still known about the thermodynamics of its fundamental steps. First principles computational studies of these dynamical

* To whom correspondence should be addressed. E-mail: wag@wag.caltech.edu.

† California Institute of Technology.

‡ Current address: Center for Neuromorphic Systems Engineering, California Institute of Technology, Pasadena, California 91125.

§ Sandia National Laboratories.

|| Current address: School of Computational Sciences, Korea Institute for Advanced Study, Seoul 130-722, Korea.

⊥ Current address: Department of Chemical Engineering, Stanford University, Stanford, California 94305.

(1) Schlier, R. E.; Farnsworth, H. E. *J. Chem. Phys.* **1959**, *30*, 917.
(2) Harrison, W. *Surf. Sci.* **1976**, *55*, 1.
(3) McRae, E. G.; Caldwell, C. W. *Phys. Rev. Lett.* **1981**, *46*, 1632.
(4) McRae, E. G. *Phys. Rev. B* **1983**, *28*, 2305.
(5) Binnig, G.; Rohrer, H.; Gerber, Ch.; Weibel, E. *Phys. Rev. Lett.* **1983**, *50*, 120.
(6) Takayanagi, K.; Tanishiro, Y.; Takahashi, M.; Takahashi, S. *J. Vac. Sci. Technol., A* **1985**, *3*, 1502.
(7) Takayanagi, K.; Tanishiro, Y.; Takahashi, S.; Takahashi, M. *Surf. Sci.* **1986**, *164*, 367.
(8) Shimada, W.; Tochihara, H. *Surf. Sci.* **2003**, *526*, 219.
(9) Shen, T.-S.; Chang, C. Y.; Chou, Y. C. *Surf. Rev. Lett.* **1999**, *6*, 97.
(10) Tromp, R. M.; Van Loenen, E. J. *Surf. Sci.* **1985**, *155*, 441.
(11) Qian, G. X.; Chadi, D. J. *Phys. Rev. B* **1987**, *35*, 1288.
(12) Khor, K. E.; Das Sarma, S. *Phys. Rev. B* **1989**, *40*, 1319.
(13) Huang, H.; Tong, S. Y.; Packard, W. E.; Webb, M. B. *Phys. Lett. A* **1988**, *130*, 166.
(14) Robinson, K. *J. Vac. Sci. Technol., A* **1988**, *6*, 1966.
(15) Ichimiya, A. *Surf. Sci.* **1987**, *192*, L893.
(16) Brommer, K.; Needels, M.; Larson, B. E.; Joannopoulos, J. D. *Phys. Rev. Lett.* **1992**, *68*, 1355.
(17) Hanada, T.; Shozo, I.; Daimon, H. *Surf. Sci.* **1994**, *313*, 143.
(18) Shigeta, Y.; Fukaya, Y. *Trends Vac. Sci. Technol.* **2001**, *4*, 1.
(19) Stelnikov, A. A.; Furthmüller, J.; Bechstedt, F. *Phys. Rev. B* **2002**, *65*, 115318
(20) Stich, I.; Payne, M. C.; King-Smith, R. D.; Lin, J.-S. *Phys. Rev. Lett.* **1992**, *68*, 1351.
(21) Bechstedt, F. Stelnikov, A. A.; Furthmüller, J.; Käckell, P. *Phys. Rev. Lett.* **2001**, *87*, 16103.
(22) Northrup, J. E. *Phys. Rev. Lett.* **1986**, *57*, 154.
(23) Northrup, J. E. In Proceedings of the Eight International Conference on the Physics of Semiconductors; Engstrom, O., Ed.; World Scientific: Singapore, 1987.
(24) Qian, G. X.; Chadi, D. J. *J. Vac. Sci. Technol., B* **1986**, *5*, 1079.
(25) Qian, G. X.; Chadi, D. J. *J. Vac. Sci. Technol.,* A **1987**, *5*, 906.
(26) Zhao, Y. F.; Yang, H. Q.; Gao, J. N.; Xue, Z. Q.; Pang, S. J. *Phys. Rev. B* **1997**, *58*, 13824.
(27) Takahashi, K.; Nara, C.; Yamagishi, T.; Onzawa, T. *Appl. Surf. Sci.* **1999**, *151*, 299.
(28) Mercer, J. L., Jr.; Chou, M. Y. *Phys. Rev. B* **1993**, *48*, 5374.

10.1021/la052029s CCC: $30.25
Published on Web 11/22/2005

processes may require unit cells many times larger than 7 × 7 (in order to describe effects such as etch pits and steps) and time scales much larger than nanoseconds. So far, the large number of atoms in the surface unit cell and the complexity of its features have impeded systematic ab initio theoretical studies, leading to significant differences in predicted energy and geometric parameters.[12,16−21,24−28] To provide a basis for developing an improved understanding of the dynamical processes on Si(111), we plan to develop a ReaxFF[29] reactive force field that will allow dynamical calculations with the thousands to millions of atoms per unit cell required to describe the formation and migration of various species and defects on the surface while also describing their reaction with adsorbed species from the gas phase. This development will require four major steps: (1) ab initio quantum mechanical (QM) characterization of all reasonable surface reconstructions with the best available methods, (2) use of these ab initio QM results to develop and train the reactive force field, (3) use of the reactive force field in molecular simulations to predict the dynamics of various *experimentally observable* surface reconstruction and reaction processes in order to validate its accuracy, and (4) application of the validated reactive force field, in molecular dynamics simulations to study new reactive processes with and without adsorbed species.

In this article, we describe the initial stage of this work. Section 2 provides a detailed description of the DAS 7 × 7 surface and an overview of 12 other relevant Si(111) surface structures. These surfaces will be used to train the reactive force field and lay the foundation for more detailed structure discussions. Section 3 describes the ab initio methods used consistently for all surfaces considered. We utilize the Perdew−Burke−Ernzerhof (PBE)[30] generalized gradient approximation (GGA) of density functional theory (DFT) whereas the local density approximation (LDA) has been employed by previous authors.[16,19−23] Section 4 presents a detailed analysis of the surface energetics and structures of the 12 Si(111) surface reconstructions and the 1 × 1 surface, all using the same level of DFT. This is the first large-scale ab inito study on Si(111) using the PBE[30] GGA to examine surface reconstructions for cell sizes up to DAS 9 × 9. Section 5.1 uses the detailed analysis of the surface reconstructions to develop the atomic energy contribution model (AECM) for partitioning the surface energy into individual atomic contributions based upon their local structural environments. This is an intermediate step between DFT and a full reactive force field. The AECM effectively reproduces the results of the DFT calculations, enabling the rapid and accurate estimation of surface energies for ordered and disordered structures. Finally, section 5.2 applies this analysis to calculate the energy of the different structures of the sequential size change (SSC) model proposed by Shimada and Tochihara[8] to describe the Si(111) DAS reconstruction path, based on real-time STM experimental observations. We find that the energy barrier in the reconstruction path is at the 2 × 2 cell and confirm that the 7 × 7 regular stage of the SSC model provides the greatest energy stabilization for the surface.

2. Si(111) Surfaces

2.1. Overview of the 7 × 7 DAS Structure. Figure 1 shows the top four layers of the DAS 7 × 7 surface reconstruction using different colors for each layer. The composite view from the top is displayed with stick (a) and ball (b) diagrams. In each case, four unit cells are shown so as to clarify the cornerhole structure. The faulted and unfaulted halves of the unit cell are distinguished by the stacking pattern. Figure 2 shows the slices for each layer of a single unit cell:

(i) The top surface layer has the 12 adatoms (purple) denoted as T_4. Each T_4 atom is bonded to three second-layer atoms (red) and has one dangling bond. In each case, there is a third-layer (dark-green) atom directly below the top atom, leading to a trigonal bipyramidal (TB) structure as indicated in Figure 3a.

(ii) The second layer (red and brown) has 42 atoms, 36 being 4-fold coordinated (red) and 6 being only 3-fold coordinated (brown). The 36 fully coordinated red atoms bond to 1 top-layer atom (purple) and 3 third-layer atoms [dark green (DG) or light green (LG)]. Of these 36, 6 atoms are bonded to 3 DG, 24 atoms to 2 DG and 1 LG, and 6 atoms to 1 DG and 2 LG. The six brown second-layer atoms bond only to three third-layer atoms (all DG), leaving a dangling bond.

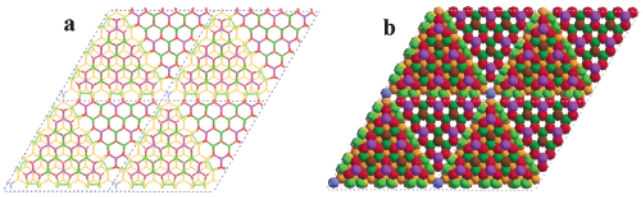

Figure 1. Top view stick (a) and ball (b) diagrams of the DAS 7 × 7 surface showing four unit cells. The top layer has 12 adatoms (purple), each with a dangling bond. At each corner is a hole centered around a dangling-bond fourth-layer atom (blue), surrounded by a 12-membered ring formed from second- and third-layer (red and light-green, respectively) atoms. The light-green atoms are third-layer dimers that connect to form eight-membered rings. The second-layer (red and brown) and third-layer nondimer atoms (dark green) form two regions, the upper right with a stacking fault and the lower left without. The brown atoms (second layer) also have one dangling bond each. The fourth layer (orange and blue) and all layers below it are unreconstructed.

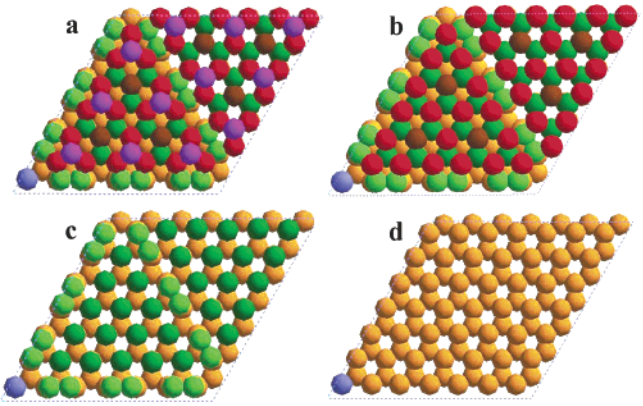

Figure 2. Top view of the DAS 7 × 7 unit cell (a) showing the top five layers, (b) upon removal of the first layer, (c) upon removal of the first two layers, and (d) upon removal of the first three layers. The top-layer adatoms (purple) correspond to the bright spots observed in STM experiments. Of the 42 atoms in the second layer (red and brown), 36 (red) are bonded to the adatoms above, but 6 (brown) are connected only to atoms in the third layer (green), leaving a dangling bond. The third-layer dimers (light green) border the left half of the unit cell. The blue atom, which occupies the center of the cornerhole, is in the fourth layer, but there is no third-layer atom above it, leading to a dangling bond. The fourth layer (orange and blue) is the first unreconstructed layer. All layers below the fourth layer are unreconstructed.

(29) van Duin, A. C. T.; Dasgupta, S.; Lorant, F.; Goddard, W. A., III *J. Phys. Chem. A* **2001**, *105*, 9396.
(30) Perdew, J. P.; Burke, K.; Ernzerhof, M. *Phys. Rev. Lett.* **1996**, *77*, 3865.

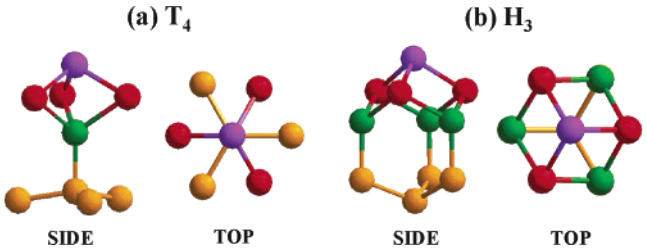

Figure 3. (a) Side and top views of a surface T_4 adatom (purple, 12 per 7 × 7 unit cell). This adatom sits on top of three second-layer atoms (red), directly above a third-layer atom (green). All adatoms in the DAS model have this structure. (b) Side and top views of a surface H_3 adatom. The adatom sits on top of three second-layer atoms (just like a T_4 adatom) but is located directly above a hollow in the subsurface. H_3 adatoms are *not* present in the DAS reconstructions.

(iii) The third layer (green) has 48 atoms:

(a) Eighteen atoms are paired to form nine dimer pairs (light green) along the edges of one of the triangles, each of which is bonded to two second-layer (red or brown) atoms, another light-green atom, and a fourth-layer atom (orange).

(b) Eighteen nondimer atoms (dark green) are bonded to three second-layer red atoms and one fourth-layer orange atom.

(c) Twelve nondimer atoms (also dark green) have the same coordination as the iii.b atoms but sit below top layer adatoms to form the bottom atom of a trigonal bipyramid as in Figure 3a.

(iv) Finally, the fourth and fifth layers of the unreconstructed bulk silicon structure (orange and blue) each have 49 atoms. One of the fourth-layer atoms (blue) has a dangling bond in the center of the 12-membered ring at the corner of the unit cell. All others are fully tetrahedrally coordinated.

The fundamental driving force for this complicated reconstruction is the removal of dangling bonds. The DAS unit cell consists of two triangular subcells. The lower left half subcell in Figure 2b leads to a surface double layer with normal sphalerite (CAABBC) stacking whereas the upper right half subcell has a stacking fault between the second (red and brown) and third (green) layers (CAABBA). The broken bonds needed to create the stacking fault are removed by forming dimers at the subcell boundary. The cell corner contains a large hole with a 12-atom ring and a dangling bond atom in the center. Holes with eight-atom rings bridge between each pair of dimers, except at the cell corners (Figure 1). The 12 top-layer adatoms each lead to a trigonal bipyramidal site (denoted T_4 because each adatom sits atop a subsurface atom and has 4 close neighbors, Figure 3a). The adatoms remove 36 dangling bonds from the second layer (leaving 6 dangling bonds) and create 12 new dangling bonds. The 12 dangling bonds from the T_4 adatoms (purple), the 6 dangling bonds from the second-layer atoms (brown), and the dangling bond from the fourth-layer atom (blue) in the cell corner lead to a total of 19 dangling bonds per unit cell in the Si(111)-7 × 7 DAS model, as opposed to the 49 dangling bonds that would be present in the unreconstructed Si(111) surface.

Despite the progress in understanding the nature of the DAS 7 × 7 structure, there remain questions regarding the relative stability of the various Si(111) reconstructed surfaces. The DAS reconstruction leads to a family of $[(2n + 1) \times (2n + 1)]$ DAS surfaces: 3 × 3, 5 × 5, 7 × 7, 9 × 9, and so forth. Of these, the 7 × 7 is the most commonly observed, although others (i.e., 5 × 5, 9 × 9, 11 × 11, etc.) have been seen on narrow terraces, quenched surfaces, and homoepitaxially grown islands as metastable states coexisting with 7 × 7 at certain temperatures.[8] Germanium, which from simple bonding considerations would be expected to yield structures similar to Si, forms a c(2 × 8) reconstruction[31] rather than a DAS 7 × 7. To understand the Si surface reconstruction fully, we need a more quantitative description of the structure and relative stabilities of the various reconstructed surfaces and of the fundamental mechanisms and parameters that drive this process.

2.2. Si(111) Surface Reconstruction Models. Here we study the following surface reconstructions.

i. 1 × 1 Unreconstructed Surface, Unrelaxed and Relaxed.

ii. √3 × √3T4. This surface contains three 1 × 1 unit cells per supercell with one adatom, leading to one dangling bond in the unit supercell. Here the adatom is bonded to 3 second-layer atoms and placed directly above a third-layer atom to form the same T_4 adatom structure as in the DAS reconstructions (Figure 3a).

iii. √3 × √3H3. This surface is similar to √3 × √3T4 except that the adatom is directly above a hollow third-layer site, leading to an H_3 site (Figure 3b).

iv. 2 × 2T4 Hexagonal. This surface contains four 1 × 1 unit cells, with one T_4 adatom (with a dangling bond) and one dangling bond atom in the second layer per supercell.

v. 2 × 2H3 Hexagonal. This is similar to a 2 × 2T4 hexagonal, except with an H_3 adatom instead of a T_4.

vi. 2 × 2T4 Rectangular. This is similar to a 2 × 2T4 hexagonal but on a rectangular cell.

vii. 2 × 2H3 Rectangular. This is similar to a 2 × 2H3 hexagonal but on a rectangular cell.

viii. 2 × 3H3T4. This surface contains six 1 × 1 unit cells per supercell and has one T_4 adatom and one H_3 adatom, leading to two dangling bonds.

ix. c2 × 8. This surface contains 16 1 × 1 unit cells per supercell with a series of 7- and 8-membered rings, 4 adatoms, and a stacking fault. This is the favored reconstruction for Ge(111) surfaces.[31]

x. DAS3 × 3: This surface has 2 T_4 adatoms, a 12-membered ring hole similar to that of the DAS 7 × 7, with a fourth-layer dangling-bond atom, 6 dimer atoms, and a stacking fault.

xi. DAS5 × 5. This surface has 6 T_4 adatoms, a 12-membered ring hole similar to that of the DAS 7 × 7, with a fourth-layer dangling-bond atom, 12 dimer atoms, 2 second-layer dangling bonds, and a stacking fault.

xii. DAS7 × 7. As described above, this surface has 12 T_4 adatoms, a 12-membered ring hole with a fourth-layer dangling-bond atom, 18 dimer atoms, 6 second-layer dangling bonds, and a stacking fault.

xiii. DAS9 × 9. This surface has 20 T_4 adatoms, a 12-membered ring hole similar to that of the DAS 7 × 7 with a fourth-layer dangling-bond atom, 24 dimer atoms, 12 second-layer dangling bonds, and a stacking fault.

3. Methods

3.1. Quantum Mechanics. Periodic ab initio calculations were performed using SeqQuest software[32] (Sandia National Laboratories, Albuquerque, NM), a DFT code for periodic and nonperiodic systems that uses contracted-Gaussian basis sets with norm-conserving pseudopotentials.[33] In all calculations, we used a well-converged

(31) Becker, R. S.; Swartzentruber, B. S.; Vickers, J. S. *J. Vac. Sci. Technol.* **1988**, *6*, 472.

(32) Schultz, P. A. *SeqQuest Electronic Structure Code*; Sandia National Laboratories: Albuquerque, NM; http://dft.sandia.gov/Quest/.

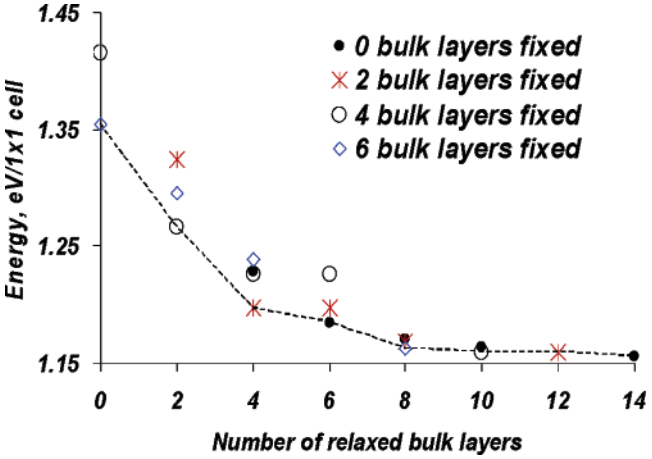

Figure 4. Minimized surface energy for the 2 × 3H3T4 surface reconstruction for various numbers of relaxed bulk silicon layers and 0 to 6 fixed bulk silicon layers below the relaxed layers. (The terminating hydrogen atoms on the bottom face were kept fixed in all geometry optimizations.) The results show that having six relaxed bulk Si layers and one fixed H layer leads to a reasonable accuracy of 0.028 eV/1 × 1 cell with respect to the converged surface energy.

double-zeta basis set with polarization functions, optimized for bulk Si, and the PBE[30] GGA with restricted (closed-shell) and unrestricted (spin-polarized) DFT. In the spin-polarized DFT calculations for systems with net spin, we carried out unrestricted calculations (i.e., those in which the N_α spin-up and N_β spin-down orbitals are optimized independently). The spin polarization is quoted in units of excess electrons of majority spin ($N_\alpha - N_\beta$) (i.e., twice the total spin projection). For net zero spin systems, we perform restricted (closed-shell) calculations where the spin-up and spin-down orbitals are taken to be identical. We cannot exclude the possibility that a net zero spin system might prefer an antiferromagnetic state instead; antiferromagnetic spin states were not examined in this study.

Nonperiodic (cluster) ab initio calculations were performed using Jaguar software (Schrödinger Inc, Portland, OR), a DFT code for nonperiodic systems that uses a variety of Gaussian basis sets (including Slater-type and Dunning-type functions) with exchange-correlation functionals ranging from LDA and GGA to hybrid functionals such as B3LYP (used in this study) and custom functionals. We used 631G**++ basis sets (double-zeta plus polarization) for all cluster calculations.

3.2. Slab Models. The surfaces were modeled using a 2D slab consisting of six layers (three double layers) of bulk silicon atoms, on top of which we formed the various reconstructed surfaces. The dangling bonds at the unreconstructed bottom surface were terminated with hydrogen atoms. These hydrogen atoms were held fixed for all geometry optimizations. The number of bulk silicon layers (six) was selected by optimizing the geometry for the 2 × 3H3T4 surface structure, increasing the total number of bulk layers (and varying the number of those layers that were held *fixed*) until the surface energy converged. Figure 4 and Table S-3 of the Supporting Information show the surface energy obtained for the 2 × 3H3T4 surface for various numbers of bulk layers and various numbers of fixed bulk layers. On the basis of this analysis, our surface slab models contain six fully relaxed silicon layers plus one termination layer of fixed hydrogen atoms. The resulting accuracy of 0.028 eV/1 × 1 cell is acceptable and applies equally to all calculations. This thickness was an effective compromise. Fewer bulk layers give insufficiently accurate surface energies, whereas more bulk layers make the calculations unnecessarily expensive. Thus, the 9 × 9 unit cell has 162 atoms per bulk double layer so that our DAS 9 × 9 model contains 739 atoms (8959 basis functions) whereas the other DAS models have 79 atoms (3 × 3), 225 atoms (5 × 5), and 445 atoms (7 × 7). In these calculations, we used the 0 K experimental lattice parameter, $a = 5.4307$ Å, for the Si bulk lattice. (For comparison, the computed PBE lattice parameter is 5.479 Å, within 1% of the experimental value.) The number of k points for each calculation was varied according to the unit cell size. For the 1 × 1 unit cell, we used 8 k points in the direction of each of the cell unit vectors. The number of k points for the other structures was set to the closest integer, inversely proportional to the cell dimension along each unit vector. Thus, the DAS 9 × 9, DAS 7 × 7, DAS 3 × 3, and 2 × 2H4 used 1, 1, 3, and 4 k points in each direction, respectively.

The normalized surface energy per 1 × 1 unit cell (E_s) is defined as follows

$$E_s = \frac{E_m - (b \times E_b) - (m \times n \times E_{H1\times1})}{m \times n} \quad (1)$$

where E_m is the minimized energy of the surface model, b is the number of silicon atoms in the model, E_b is the energy per silicon atom in the bulk crystal, $m \times n$ is the size of the unit cell in terms of 1 × 1 unit cells, and $E_{H1\times1}$ is the energy change per hydrogen obtained when adding a hydrogen atom to the unreconstructed 1 × 1 unit cell to form a hydrogen-terminated 1 × 1 surface. This term was obtained from a 20-bulk-layer 1 × 1 silicon slab terminated with hydrogen atoms on both faces.

4. Si(111) Surface Reconstructions: Density Functional Calculations

4.1. Energetics. The results of our DFT calculations of surface formation energies (with respect to the bulk crystal) of different Si(111) surface reconstructions are presented in Table 1, along with previous DFT results. Of all of the surfaces we considered, we find that the DAS 7 × 7 reconstruction gives the lowest surface energy (1.044 eV/1 × 1 cell), followed by the DAS 5 × 5 (1.048 eV/1 × 1 cell), and then the DAS 9 × 9 (1.055 eV/1 × 1), in general agreement with the work of previous authors.[19−21,24−27] Relevant to the SSC model,[8] we identify a barrier in the reconstruction path of 0.23 eV/1 × 1 cell at the 2 × 2 cell size. The results confirm that the 5 × 5 and 7 × 7 regular stages of the model, which correspond to the DAS 5 × 5 and 7 × 7 reconstructions, provide the greatest energy reduction with respect to the unreconstructed 1 × 1 surface. The optimal reconstructed surface (DAS 7 × 7) is calculated to be ~0.16 eV/1 × 1 cell below the unreconstructed (relaxed) 1 × 1 Si(111) surface.

The PBE functional used in the current study does not give qualitatively different results in comparison to the LDA functional used in previous studies. Quantitatively, our predicted surface formation energies for all DAS surface models (including the DAS 7 × 7 structure) are lower than others in the literature. A comparison of LDA and PBE[30] surface energies for cell sizes up to 3 × 3 (Table S-4 in the Supporting Information) gave values that were on average 0.152 eV/1 × 1 cell *higher* when using LDA than when using PBE. This trend was observed in all calculations. The largest difference (0.250 eV/1 × 1 cell) was observed for the 1 × 1 relaxed surface, and the smallest difference, for the 2 × 2H3 surface (0.114 eV/1 × 1 cell).

(33) Hamann, D. R. *Phys. Rev. B* **1989**, *40*, 2980.

Table 1. First Principles Surface Energies for Si(111) Surfaces[a]

surface	this work	Stelnikov et al. (2002)[19]	Bechtedt et al. (2001)[21]	Stich et al. (1992)[20]	Brommer et al. (1992)[16]	Northrup (1986)[22,23]
method	PBE−DFT	LDA−DFT	LDA−DFT	LDA−DFT	LDA−DFT	LDA−DFT[c]
1 × 1 unrelaxed	1.224	1.435	0 (ref)[b]			0 (ref)[b]
1 × 1 relaxed	1.200	1.372				−0.17
$\sqrt{3} \times \sqrt{3}$H3 hex	1.353					−0.067
$\sqrt{3} \times \sqrt{3}$T4 hex	1.102					−0.28
2 × 2H3 hex	1.209					−0.24
2 × 2T4 hex	1.083					−0.24
2 × 2H3 rect	1.264					−0.17
2 × 2T4 rect	1.085					
2 × 3H3T4	1.184					
c2 × 8	1.184	1.109	−0.33			
DAS3 × 3	1.070			1.196		
DAS5 × 5	1.048			1.168		
DAS7 × 7	1.044	1.073	−0.36	1.153	1.179	
DAS9 × 9	1.055					

[a] Energies are eV per 1 × 1 unit cell. The reference energy is zero for the bulk crystal unless otherwise indicated, in which case the reference energy is the unrelaxed 1 × 1 unreconstructed surface. [b] Absolute energies not provided. [c] Cluster calculations.

Thus, we attribute the difference between our results and those of other authors primarily to the use of the PBE functional instead of the LDA functional.

The formation energy of the relaxed unreconstructed 1 × 1 Si(111) surface is computed to be 1.20 eV. Attributing this surface energy solely to the breaking of bonds at the surface (a crude but not unreasonable first approximation), this corresponds to each dangling bond adding 1.20 eV to the formation energy. Using this value, we can analyze the contribution of the dangling bonds to the surface energy of the DAS 7 × 7 reconstruction. Consider a 7 × 7 supercell of the 1 × 1 surface. For the unreconstructed supercell, the 49 broken bonds incur a total energy cost of 58.8 eV (49 dangling bonds costing 1.20 eV each). As discussed above, the DAS 7 × 7 structure eliminates 30 of these dangling bonds, leaving only 19 dangling bonds. Ideally, this would stabilize the surface by 36.0 eV (30 × 1.20 eV). The computed stabilization, however, is only 7.65 eV (0.26 eV per dangling bond removed). Although the elimination of the dangling bonds may be the principal driving force for the reconstruction, the strain introduced in the reconstruction plays an important role and significantly reduces the net stabilization given by the elimination of dangling bonds.

Table S-5 of the Supporting Information compares the calculated surface energies for the different Si(111) reconstructions (with respect to the bulk crystal) to previously published empirical and semiempirical results, indicating the method used in each case. Our results qualitatively agree with those of Zhao et al.,[26] who used a building block energy contribution model, and those of Takahashi et al.,[27] who used a modified embedded atom model.

Because all surface models of Si(111) contain dangling bonds and because these dangling bonds are unable to make good bond pairs, it is plausible that the surface might have unpaired spins. We performed a series of spin-polarized calculations to examine whether the surface might prefer to have net spin rather than be closed shell. The $\sqrt{3} \times \sqrt{3}$ and 1 × 1 surfaces have one dangling bond per supercell. For these two surfaces, the lowest-energy state was indeed found to have net spin, with a net spin polarization of one electron per supercell. For all other surfaces examined (2 × 2, 2 × 3, 2 × 8, 3 × 3, 5 × 5, and 7 × 7, except 2 × 2H3 rect, which was found to have a net spin of two electrons per supercell), the spin-zero closed-shell state was the ground state (Table S-6 of the Supporting Information). We varied the spin from zero to a maximum in which all dangling-bond electrons were ferromagnetically aligned. Figure 5 displays the computed surface energy of the DAS 5 × 5 surface as a function of the net spin polarization. The results are characteristic of the results for the other reconstructed surfaces. The surface energy is lowest for the spin-zero case and increases monotonically with increasing number of unpaired electrons. Similar calculations were performed for DAS 3 × 3 and for the lowest five and the highest spin states of DAS 7 × 7. (The results are provided in Tables S-7, S-8, and S-9 and Figures S-1 and S-2 of the Supporting Information.) We did not perform the unrestricted spin calculations for the DAS 9 × 9 structure but expect that the ground state will also have no net spin.

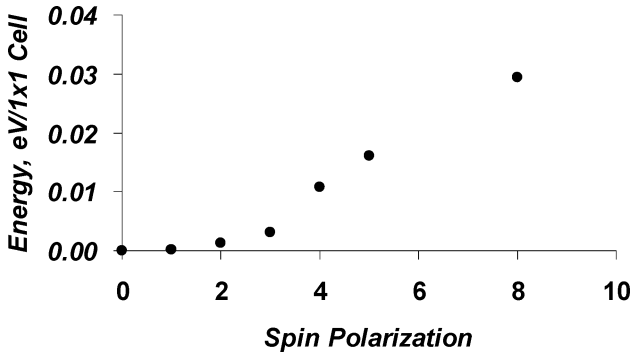

Figure 5. Surface energy for the DAS 5 × 5 surface model as a function of the spin polarization (number of electrons with unpaired spins). The results show that the surface energy is at a minimum when there are no unpaired spins (spin polarization zero). Similar trends were calculated for the DAS 3 × 3 and the DAS 7 × 7 models and for most of the 2 × 2, 2 × 3, and 2 × 8 structures analyzed (Supporting Information). Note that the DAS 5 × 5 surface contains nine dangling bonds.

4.2. Energetics for H_3 and T_4 Adatoms. Because there are two possibilities for the local structure of the adatoms, H_3 and T_4 (Figure 3), and because only T_4 adatoms are observed in the DAS structures, we considered it necessary to investigate the fundamental differences between the two adatom types, which lead to the observed preference. Table 1 shows that the calculated surface energies of the $\sqrt{3} \times \sqrt{3}$H3 and $\sqrt{3} \times \sqrt{3}$T4 structures are 1.353 eV/1 × 1 cell and 1.102 eV/1 × 1 cell respectively, indicating that the $\sqrt{3} \times \sqrt{3}$H3 surface is *not* as stable as the 1 × 1 unreconstructed surface whereas the $\sqrt{3} \times \sqrt{3}$T4 surface is nearly as stable as the DAS structures. Both surfaces contain one dangling bond per unit cell, and in both cases the adatom sits on top of three unreconstructed silicon atoms, which would otherwise form a 1 × 1 unrecon-

Table 2. $\sqrt{3} \times \sqrt{3}$H3 and $\sqrt{3} \times \sqrt{3}$T4 Electronic Structure and Geometry Calculations[a]

	$\sqrt{3} \times \sqrt{3}$H3	$\sqrt{3} \times \sqrt{3}$T4	$T_4 - H_3$ difference
surface energy	4.059	3.307	−0.751
surface strain energy (below adatom)	0.351	0.607	0.256
stabilization due to bonding hydrogen to dangling bond	−3.122	−3.165	−0.043
stabilization due to adatom snap bond energy	−4.601	−5.594	−0.993
adatom bond angle, deg	87.9	87.6	−0.3
adatom bond length, Å	2.59	2.51	−0.08

[a] All energies are eV per $\sqrt{3} \times \sqrt{3}$ unit cell.

structed surface. The only difference between them is that the H_3 adatom sits above a void in the subsurface layer and the T_4 adatom sits directly above a subsurface atom.

To understand these differences better, we performed a series of calculations on both surfaces as follows (the results are summarized in Table 2):

i. Bond Energy of Hydrogen to the Adatom. For this calculation, we bonded a hydrogen atom to the dangling bond of the adatom and computed the bond energy while keeping the Si atoms fixed (optimizing only the H atom). Here we found similar bond energies (3.122 eV for $\sqrt{3} \times \sqrt{3}$H3 and 3.165 eV for $\sqrt{3} \times \sqrt{3}$T4). This suggests that the dangling-bond electron has similar character for both and does not participate differentially in any bonds to subsurface atoms.

ii. Surface Strain Energy upon Removal of the Adatom without Relaxation. Here we removed the adatom from the optimized $\sqrt{3} \times \sqrt{3}$H3 and $\sqrt{3} \times \sqrt{3}$T4 surfaces without relaxation, did a single-point energy calculation, and subtracted from it the *relaxed* unreconstructed Si(111) surface energy. This snap strain energy is 0.36 eV for H_3 and 0.61 eV for T4, indicating that the T_4 adatom causes *more* strain in the initial relaxed (111) structure.

iii. Adatom Snap Bond Energy. This is the difference in energy between the optimized surface structure and the resulting *unrelaxed* surface structure obtained when the adatom is displaced to infinity with all other atoms kept fixed. The calculated snap bond energies are 4.60 eV for $\sqrt{3} \times \sqrt{3}$H3 and 5.59 eV for $\sqrt{3} \times \sqrt{3}$T4. This is the most substantial difference (1.0 eV), indicating that electronic effects are important.

iv. Bonding Si to the Normal Site. This is the bond energy of a single Si atom on top of a single 1×1 surface atom. This leads to one dangling-bond π orbital and one lone pair on the Si adatom. The calculated bond energy is 2.257 eV, significantly lower than the snap bond energy of the H_3 and T_4 adatoms. This result shows that it is important for the adatom to bend over toward the surface and form three bonds.

These calculations show that the difference in surface energy for $\sqrt{3} \times \sqrt{3}$T4 versus $\sqrt{3} \times \sqrt{3}$H3 cannot be explained by differences in subsurface strain or in the character of the bonds formed by the dangling-bond electron alone. Instead, the large difference in snap bond energy of 1 eV indicates that the more favorable surface energy of $\sqrt{3} \times \sqrt{3}$T4 is primarily due to electronic effects associated with forming bonds between the adatom and the 1×1 subsurface.

There are two differences in the bonds formed by the T_4 and H_3 adatoms, which favor the H_3 configuration. The first of these is the Pauli repulsion between the adatom (purple) and the second-layer atom located 2.50 Å directly below it (green) in the T_4 surface, which does not take place in the H_3 structure (Figure 3). This effect is not directly quantifiable, but our calculations show that it causes the green atom to move downward by ~0.61 Å, which could be significant. The second effect favoring H_3 is the difference in the bond angle strain of the red atom due to the new bond with the adatom (this is *not* included in the subsurface strain result of Table 2). We estimated its magnitude by performing DFT cluster calculations (using the 631G**++ basis set) on an SiH_4 molecule having the same bond angles as a 1×1 red atom with an additional bond in the H_3 or T_4 configuration and obtained an energy difference of ~0.13 eV for every three atoms bonded to one adatom.

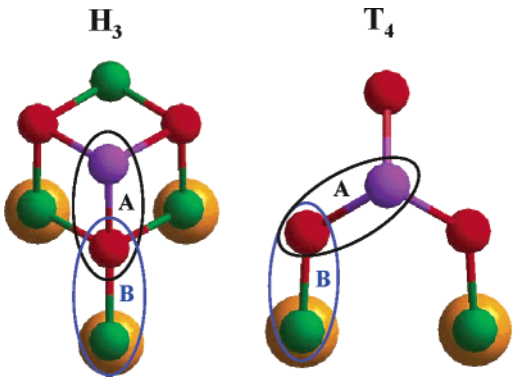

Figure 6. Top view of the orientation of the H_3 and T_4 adatom bonds with respect to those of the unreconstructed surface. The picture shows that the bonds between the adatom and the second-layer atoms (A), the bonds between the second- and the third-layer atoms (B), and the bonds between the third- (green) and fourth- (orange) layer atoms are all approximately in the same plane for H_3 adatoms but not for T_4.

There are also two differences in bonding, which favor the T_4 configuration. The first one can be understood by looking at the new bonds that need to be formed upon placement of the adatom in each case. Figure 6 illustrates the orientation of the bonds between the adatoms and the second-layer atoms (labeled A) with respect to the bonds between the second- and third-layer atoms (labeled B). Adding an H_3 or T_4 adatom to the 1×1 unreconstructed surface requires the formation of three new A bonds. A geometrical analysis of the $\sqrt{3} \times \sqrt{3}$H3 surface reveals that the A and B bonds and the bonds between the third (green) and fourth (orange) layers (denoted C) are all in the same plane, which leads to slightly repulsive interactions resulting from orthogonalizing these three bonds with respect to one another. In contrast, in the $\sqrt{3} \times \sqrt{3}$T4 surface, the A bond points in a direction 60° away from the B bond (when observed from above) so that it *cannot* be in the same plane as the B and C bonds, and the coupling is more favorable than in $\sqrt{3} \times \sqrt{3}$H3. The energy difference between these two cases cannot be calculated directly using DFT, but we expect it to be of the same order of magnitude as the energy cost of introducing a stacking fault between the first and second layers of the unreconstructed 1×1 surface (calculated to be ~0.048 eV/cell), which changes the Si−Si−Si−Si torsion angle of the atoms in the top four layers from 60 to 0°. However, when compared to the 1 eV difference in bond energy between H_3 and T_4 adatoms, this effect is very small. A much more important factor explaining the strong preference for the T_4 structure is the delocalization of the dangling-bond orbitals into the subsurface layers, which allows the dangling-bond orbital (HOMO) to be partially stabilized by using some LUMO character from the C bond that is aligned with the adatom. Figure 7 shows that electronic delocalization is significant in the T_4 structure, with HOMO density in the third and fourth layers. This

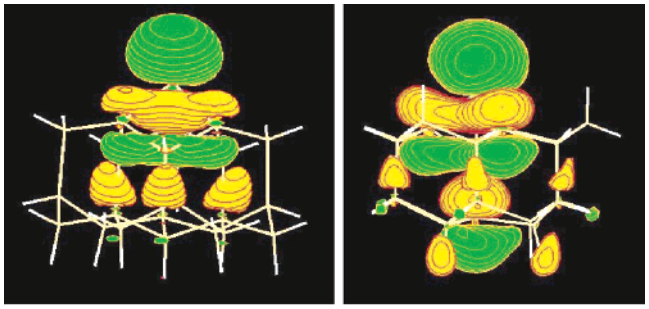

Figure 7. Highest occupied molecular orbital (HOMO) for clusters containing a single H_3 or T_4 adatom. This is the dangling-bond orbital with just one electron. Obvious here is the greater electronic delocalization for the T_4 adatom, with significant density in the third and fourth layers. These calculations used 631G**++ basis sets and the B3LYP functional.

cannot occur for H_3 because the adatom sits above a hollow and is not aligned with any of the C bonds. None of the factors discussed above can be considered in isolation, so it is *not* possible to estimate the HOMO delocalization energy in the T_4 surface by simply adding all other contributions. However, if we neglect the small energy difference in the orientation of the adatom bonds illustrated in Figure 6 and consider that the HOMO delocalization effect must compensate for the difference in bond angle strain, subsurface bond strain, bond energy, and Pauli repulsion, then we can expect it to be on the order of ~1−1.2 eV.

4.3. Geometry Analysis of the DAS 7 × 7 Reconstruction. The total energy calculations for the DAS 7 × 7 reconstructed surface indicate that forming this structure leads to ~28.35 eV of strain per 7 × 7 cell. The strain is evident when one considers the significant deviations in geometry with respect to the bulk structure in terms of atomic layer vertical positions, bond lengths, and bond angles. In this section, we examine the details of the optimized 7 × 7 structure to gain a better understanding of the strain that exists in the structure and lay the foundation for the next section, where we decompose the energy of a reconstructed surface into contributions of different atom types.

4.3.1. Crystal Layer Positions. Table 3 provides the calculated vertical positions of the different layers in the DAS 7 × 7 surface (a side view illustrated in Figure 8) and compares them to the bulk structure. Consider first dangling-bond atoms 1, 2, and 8. In bulk silicon, the vertical distance separating a double layer is 0.784 Å. In the DAS 7 × 7 reconstruction, atoms 1, 2, and 8 are respectively 1.340, 1.113, and 1.277 Å above the next layer. This is much larger than the bulk value, indicating that significant strain is present, although not as great as that present in the pure T_4 adatoms of the $\sqrt{3} \times \sqrt{3}$T4 structure, which are 1.507 Å above the next layer. Now consider the vertical position of the atoms in the third (green) layer. Because of the presence of atom 1, atom 6 is displaced 0.607 Å lower than atom 4. Atom 5 (a dimer atom adjacent to the cornerhole) is not located below an adatom, but it is also lower than atom 4 by 0.241 Å. As a result of the downward shifting of atom 6, atom 9, located immediately below, is also displaced downward by approximately 0.333 Å with respect to the bulk structure.

Table 3 also compares our results to other first principles and experimental results available in the literature. Our results compare well with the experimental results of Shigeta and Fukaya,[18] who used reflection high-energy electron diffraction (RHEED). The most significant differences are the vertical positions of atom 8 (our result is 0.520 Å higher) and the vertical position of atom 9 (our result is 0.188 Å lower). Our results are in moderate agreement with the ab initio results of Stelnikov et al.[19] and Brommer et al.,[16] which were based on LDA rather than PBE calculations. The differences may also be related to the periodicity of the model and the type of basis set. (Their calculations used plane wave basis set and 3D periodic supercell models with vacuum space between the slabs, whereas we used Gaussian basis sets and 2D periodic models.)

4.3.2. Bond Lengths. Table 4 provides the bond lengths in the reconstructed surface layers of the DAS 7 × 7 surface for different types of atom pairs. Most of them exhibit bond lengths that are *longer* than the experimental bulk value of 2.352 Å, except for the bonds between atoms 6 and 9 and between atom 9 and the bulk layers below, which are shorter as a consequence of the vertical displacements in the third layer caused by the adatom. A key parameter in the DAS 7 × 7 model is the nonbond distance between the adatom and the subsurface atom below it (atoms 1 and 6, respectively, in Figure 8). Proposed values of this distance have ranged from 2.45 to 3.1 Å, reflecting the uncertainty remaining in the structure characterization. The value obtained from our periodic ab initio calculations ranged from 2.48 to 2.54 Å depending upon the site within the surface reconstruction. The Si−Si dimer bond length is another important distance, for which our calculated values range from 2.43 to 2.46 Å depending upon the site. This agrees well with the LDA DFT calculations of Stelnikov et al.[19] (2.442 Å) and Stich et al.[20] (2.446 Å).

4.3.3. Bond Angles. Table 5 shows that there are also significant deviations in the bond angles with respect to the tetrahedral bulk structure (109.4°). The most dramatic deviations are the bond angles of the T_4 adatoms (94.2°), which sit directly above a subsurface atom, and the bond angles between atoms 6, 3, and 5 (95.5°), which are reduced by the downward displacement of atoms 5 and 6, as discussed above. The bond angle centered on atom 2 (100.8°) is also significantly *less* than tetrahedral, indicating that the character of the dangling bond on this atom is different than that of a relaxed 1 × 1 site, which has a bond angle (110.4°) slightly *greater* than the tetrahedral angle of the bulk structure. The other dangling-bond atom (8) has bond angles (114.1°) significantly larger than those of the 1 × 1 relaxed structure (this atom belongs to an unreconstructed bulk layer and would be expected to behave similarly to the 1 × 1 surface atoms). Finally, consider atoms 7 and 9. Atom 7 has average bond angles close to the bulk value (107.9°) but exhibits significant variability depending on location. Because of its significant downward displacement, atom 9 has the largest bond angles (115.6°). This analysis points out that the strain present varies greatly across the different atom types in the reconstruction and motivates the energy decomposition chosen for defining the AECM in the next section.

5. Atomic Energy Contribution Model (AECM)

5.1. Energy Partitioning. To understand the relevant contributions to the surface energy better, we classified each surface atom in terms of its local environment using seven types (listed in Table 6). Then we assumed that each type of atom contributes a certain increment to the average surface energy, proportional to a power of its average number density (per 1 × 1 cell) *independent* of the specific surface structure it is embedded in, as

Table 3. Vertical Layer Position (Å) for the DAS 7 × 7 Structure Obtained from PBE Calculations[a]

layer	bulk crystal	this work	Shigeta and Fukaya (2001)[18]	Hanada et al. (1994)[17]	Stelnikov et al. (2002)[19]	Brommer et al. (1992)[16]
method	N/A	PBE−GGA	RHEED[b]	RHEED[b,c]	LDA	LDA
L1	6.271	5.275	5.281	L2 + 0.67	L3 + 1.309	5.148
L2	3.919	4.486	4.415			4.173
L3	3.919	3.935	3.853	L2 − 0.54	L2 − 1.108	3.814
L4	3.125	3.373	3.331			3.221
all dimers	3.135	3.154				
L5	3.135	3.132	3.026	L4 − 0.14		3.081
L6	3.135	2.766	2.699	L4 − 0.48		3.045
L7	0.784	0.887	0.928			0.811
L8	0.784	1.277	0.757			0.788
L9	0.784	0.454	0.642	L7 − 0.34	1.129	0.445

[a] The numbers correspond to the atomic vertical positions with respect to the fifth (unreconstructed) layer, as shown in Figure 8. Also shown are comparisons to previously published results. The results of Stelnikov et al.[19] and Hanada et al.[17] use different reference layers as indicated. [b] Reflection high-energy electron diffraction. [c] Average values for faulted and unfaulted atoms.

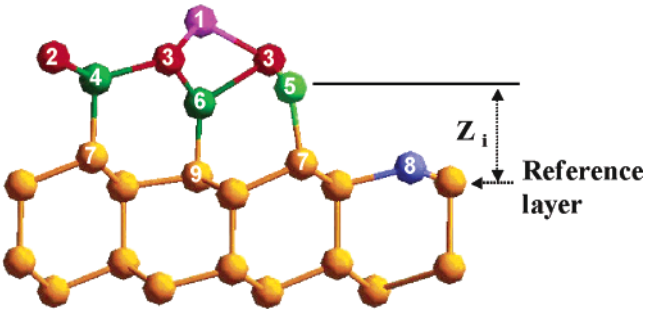

Figure 8. Atom positions corresponding to the dimensions given in Tables 3, 4 and 5. The fourth and fifth (reference) layers are unreconstructed. Atom 8 is the cornerhole atom.

Table 4. Average Bond Length for Selected Pairs of Atoms of the DAS 7 × 7 Structure from PBE Calculations[a]

atom pair		bond length, Å	deviation from experimental bulk, Å
bulk	bulk	2.352	N/A
bulk	1 × 1 relaxed	2.352	∼0
1	3	2.485	0.133
1	6[b]	2.504	0.152
2	4	2.416	0.064
3	4	2.424	0.072
3	5	2.475	0.123
3	6	2.394	0.042
4	7	2.431	0.079
5 (dimer)	5 (dimer)	2.449	0.097
5	7	2.408	0.056
6	9	2.312	−0.040
7	bulk	2.372	0.020
8	bulk	2.389	0.037
9	bulk	2.341	−0.011

[a] All atom numbers correspond to those of Figure 8, except for those of the 1 × 1 surface atom. [b] Adatom nonbond distance.

described by the following equation

$$E_s = \sum_{i=1}^{7} C(i)\ \rho(i)^{\exp(i)} \qquad (2)$$

where E_s is the average surface energy per 1 × 1 cell, $C(i)$ and $\exp(i)$ are the coefficient and exponent corresponding to atom type i, respectively, and $\rho(i)$ is its average number density per 1 × 1 cell. This is similar to the model used by Zhao et al.[26] but is based on feature densities instead of absolute energy contributions and on individual atom features instead of larger structural units. It also introduces exponents for the average feature density, thus allowing for nonlinear relaxation effects as described below.

Table 5. Bond Angle Averages and Ranges for Selected Atoms of the DAS 7 × 7 Structure from PBE Calculations[a]

atoms forming bond angle	average bond angle, deg	bond angle range, deg
bulk-1 × 1-bulk relaxed	110.4	N/A
bulk−bulk−bulk	109.4	N/A
3−1−3	94.2	91.3−96.3
4−2−4	100.8	98.7−103.0
4−3−6	106.8	105.3−107.9
6−3−5	95.5	95.4−95.5
ref−7−ref	107.9	101.7[b]−112.5[c]
ref−8−ref	114.1	N/A[d]
ref−9−ref	115.6	113.7−117.2

[a] All atom numbers correspond to those of Figure 8, except for those of the 1 × 1 surface atom. [b] This angle occurred under atom 4, near the cornerhole. [c] This angle occurred under atom 5, at the cornerhole. [d] There is only one bond of this type in the unit cell.

Table 6. Fitted Coefficients and Exponents by Atom Type for the AECM

atom type, i	coefficient, C(i)	exponent, exp(i)
atom corrections		
1 × 1 dangling-bond atom (1 × 1)	1.2004 (DFT result)	1
H_3 adatom (H3)[b]	3.8933	1
T_4 adatom (T4)	3.2264	1
dimer atom (D)	0.9936	1
configuration corrections		
8-membered ring atom (8R)	−0.2617	1.2865
12-membered ring atom (12R)	−0.3133	1.3267
atom in a faulted position (F)	0.0482 (DFT result)	1

[a] Note that atoms classified as F or D may also belong to other types simultaneously. (For example, all D atoms in the DAS7 × 7 model are also classified as either 8R or 12R. Both contributions must be added to the total surface energy.) Atoms shared by more than one ring were assigned to the largest ring. [b] This atom type is not present in the DAS structures.

The energy contributions of two of the atom types in Table 6—the 1 × 1 surface atom with a dangling bond and the atom at a faulted position—were obtained directly from DFT calculations on a 1 × 1 unit cell and were assumed to have an exponent of 1 in the expression for E_s. The remaining energy terms were fitted to the ab initio surface energies according to the atom-type composition for each surface given in Table 7 in order to obtain their coefficients and exponents (listed in Table 6). We found that exponents different from unity were necessary only for atoms types 8R and 12R (belonging to 8- and 12-membered rings, respectively), whose fitted coefficients are negative, indicating that these configurations help stabilize the surface *in the presence of the other types of atoms*, suggesting that they may play an important role in surface

Table 7. Average Atom Type Composition per 1 × 1 Cell for the Si(111) Surface Reconstructions Used in the Construction of the AECM[a]

surface	1 × 1	H3	T4	8R	12R	F	D
√3 × √3T4 hex	0	0	1/3	0	0	0	0
√3 × √3H3 hex	0	1/3	0	0	0	0	0
2 × 2T4 hex	1/4	0	1/4	0	0	0	0
2 × 2T4 rect	1/4	0	1/4	0	0	0	0
2 × 2H3 hex	1/4	1/4	0	0	0	0	0
2 × 2H3 rect	1/4	1/4	0	0	0	0	0
2 × 3H3T4	0	1/6	1/6	0	0	0	0
c2 × 8	0	0	4/16	16/16	0	6/16	10
DAS3 × 3	1/9	0	2/9	0	12/9	3/9	6/9
DAS5 × 5	3/25	0	6/25	24/25	12/25	10/25	12/25
DAS7 × 7	7/49	0	12/49	48/49	12/49	21/49	18/49
DAS9 × 9	13/81	0	20/81	72/81	12/81	36/81	24/81
DAS11 × 11	21/121	0	30/121	96/121	12/121	55/121	30/121
DAS13 × 13	31/169	0	42/169	120/169	12/169	78/169	36/169
DAS infinite	0.25	0	0.25	0	0	0.5	0

[a] Each fraction corresponds to the number of features present in the supercell (of size $n \times n$) divided by n^2. For the *infinite* DAS model, the numbers correspond to the average fraction of atoms of each type per 1 × 1 cell.

Table 8. Surface Energies Estimated Using the AECM and Deviations from the Ab Initio Results

	atom type corrections, eV/1 × 1 cell	configuration corrections, eV/1 × 1 cell	total surface energy/ 1 × 1 cell	error vs ab initio result, eV/ 1 × 1 cell
1 × 1 relaxed	1.200	0	1.200	0
√3 × √3T4 hex	1.075	0	1.075	−0.027
√3 × √3H3 hex	1.298	0	1.298	−0.055
2 × 2T4 hex	1.107	0	1.107	0.024
2 × 2T4 rect	1.107	0	1.107	0.022
2 × 2H3 hex	1.273	0	1.273	0.064
2 × 2H3 rect	1.273	0	1.273	0.007
2 × 3H3T4	1.187	0	1.187	0.003
c2 × 8	1.428	−0.244	1.184	$<10^{-3}$
DAS3 × 3	1.513	−0.443	1.070	$<10^{-3}$
DAS5 × 5	1.395	−0.347	1.048	$<10^{-3}$
DAS7 × 7	1.327	−0.283	1.044	$<10^{-3}$
DAS9 × 9	1.284	−0.228	1.055	$<10^{-3}$
DAS11 × 11	1.255	−0.187	1.068	N/A
DAS13 × 13	1.234	−0.156	1.078	N/A
DAS infinite	1.107	0.024	1.131	N/A

relaxation. (Such a negative energy contribution does not mean that the configuration is more stable than the bulk diamond structure but only that it contributes to the stability of the reconstructed system containing the strain of various dangling-bond configurations.)

The calculated surface energies using this model and quality of fit with respect to the ab initio results are given in Table 8. The results show that despite its simplicity the AECM approximation is remarkably good with errors of <0.1% for the formation energy of the DAS structures as shown in Figure 9. This Figure also shows that the AECM surface energy of the DAS reconstructions increases monotonically for unit cells larger than 7 × 7 but that the slope becomes gradually smaller as the unit cell size (n) increases. This indicates that the surface energy of DAS models levels off very quickly as a function of n. Extrapolating our AECM surface energy calculations to an infinitely large DAS model (Figure 10), we obtain an energy of 1.131 eV/1 × 1 cell, lower than the calculated surface energy of the unreconstructed 1 × 1 surface (1.200 eV/1 × 1 cell). This infinite case is dominated by the large triangular regions of adatoms and exposed second-layer atoms (purple and brown, respectively, in Figures 1 and 2) leading to a surface that resembles the 2 × 2T4 structure but with a stacking fault as in all DAS models.

Figure 10 shows the normalized atom energy contributions for DAS [(2n + 1) × (2n + 1)] structures plotted

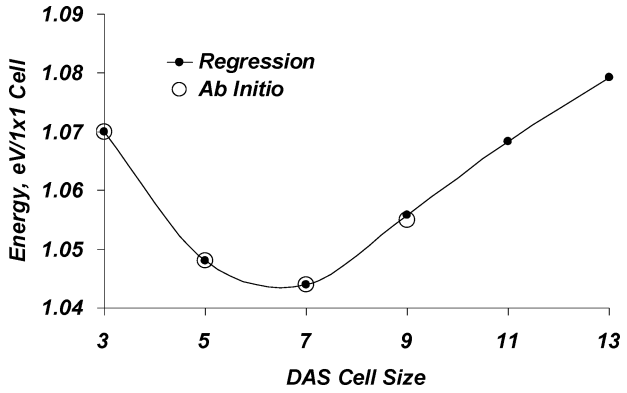

Figure 9. Ab initio and AECM surface energies for the DAS surfaces from 3 × 3 to 13 × 13. The black open circles are the ab initio results, and the dots represent AECM calculations. The graph shows good agreement between the two.

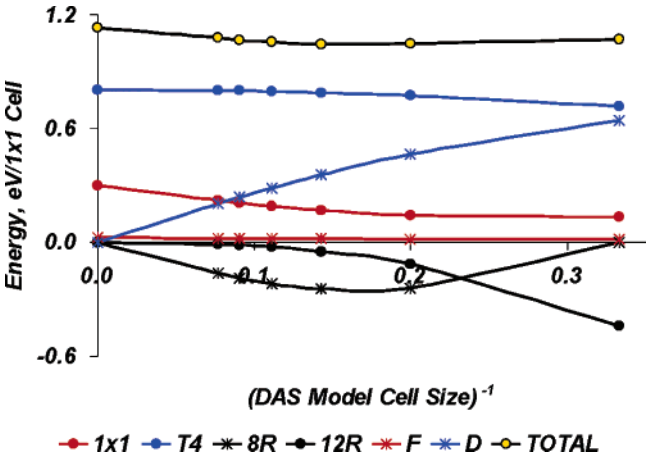

Figure 10. Atom type energy contributions as a function of n^{-1} for DAS [(2n + 1) × (2n + 1)] models between 3 × 3 and infinity. The atom type labels and descriptions are the same as in Table 6. The graph shows that the differences between different values of n vanish when n grows to infinity (i.e., when n^{-1} approaches zero). It also shows that the DAS surface energy reaches an asymptotic value in the limit of very large unit cells ($n^{-1} = 0$), calculated to be 1.131 eV/1 × 1 cell.

versus n^{-1}. As n increases (i.e., as n^{-1} approaches zero), these contributions converge to a constant value, which, as indicated above, adds up to 1.131 eV/1 × 1 cell. The number of all surface features increases linearly as n, except for the area of the faulted and unfaulted triangular regions, which increases as n^2 (and becomes dominant at very large cell sizes).

Finally, we must note that the AECM does *not* capture the energy differences between cells of different geometry containing the same density of surface features, such as the 2 × 2H3 hexagonal and rectangular surfaces for which the same energy is predicted. (The energy differences between the 2 × 2H3 and T4 hexagonal and rectangular surfaces are primarily a result of different adatom bond and subsurface strain energies and are discussed in more detail in the Supporting Information.) Nonetheless, the AECM is sufficiently accurate to analyze general trends in surface reconstruction and allows the rapid estimation of the energy for both periodic and nonperiodic systems. The next section applies this analysis to the real-time reconstruction process of the Si(111) 1 × 1 surface observed by Shimada and Tochihara[8] using STM.

5.2. Application of the AECM to Real-Time Reconstruction Observations. Shimada and Tochihara[8] recently reported real-time observations of the 1 × 1 Si(111) reconstruction process using STM. They determined

surface structures for the different stages of reconstruction of the faulted half of the DAS unit cell for various cell sizes. They propose the SSC model, in which surface reconstruction depends primarily on the reconstruction path of the faulted half of the unit cell. Their experimental observations show that the unit cell grows according to a zipperlike pattern that displaces the row of dimers around the unit cell one cell at a time. To determine the reaction energy profile and to compare the results to the calculated surface energy of the different sizes of DAS models, we applied the AECM to the different structures of the SSC.

We started with a periodic cell having a 16 × 16 array of 1 × 1 cells of the unreconstructed surface. We then modified the structure according to the different stages of the SSC model.[8] For each stage, we determined the average density per 1 × 1 cell of atoms of each type (listed in Table 6) and calculated the average surface energy *in the reconstructed region* and the total energy of the 16 × 16 supercell. (The energy of the unreconstructed part of the supercell can be easily calculated using the surface energy of the 1 × 1 relaxed surface.) Because the SSC model contains additional structural components that are similar but not identical to those listed in Table 6 and because the size of the reconstructed region is not obvious for each stage, we defined the following rules for the application of the AECM:

(i) Seven-membered rings are not included in the calculation of the surface energy. (These rings are present in the c2 × 8 reconstruction, but the regression analysis performed in constructing the AECM shows that it is not necessary to assign them an energy contribution.)

(ii) All atoms containing dangling bonds, which are in the same layer as the surface atoms in the unreconstructed region, are classified as 1 × 1 atoms (faulted or unfaulted).

(iii) Atoms with dangling bonds on the step edges of incomplete cornerholes are treated as 1 × 1 unfaulted atoms. (They are tetrahedral and are not subject to strain, just like regular 1 × 1 atoms.)

(iv) Atoms that would be classified as 12R in a perfect cornerhole are treated as 12R atoms (there are 6 in each irregular-odd and 3 × 6 = 18 in each regular-odd SSC structure).

(v) Finally, to compute the feature densities, it is necessary to define the size of the reconstructed region, which we calculated as $[n^2/2 + (n + 2) \times (n + 2)/2]$, except for the 2 × 2 cell whose size was assigned as $[n^2/2 + (n + 2) \times (n + 2)/2 + 1]$. This is approximately equal to the size of the faulted half plus half of a unit cell two sizes larger and was estimated on the basis of the area occupied by the reconstructed half, the band of adatoms surrounding it, and the atoms below these adatoms.

Figure 11 compares the ab initio surface energy of each *n*-sized periodic DAS structure to the average surface energy of the reconstructed region of the corresponding SSC stage. We see that the energy of the SSC regular-odd structures, which lead to DAS structures, shows a minimum at the 7 × 7 cell size, in agreement with the DFT result. The energy of the irregular-odd and even SSC structures is nonmonotonic and has local minima at the 6 × 6 and 8 × 8 cell sizes. This curve also exhibits a reaction barrier at the 2 × 2 cell size and local barriers between *adjacent* even cell sizes. Although the average surface energy for the irregular-odd and even SSC structures is slightly lower than that of the regular-odd structures, the latter are favored in an infinite domain because the former are *not* able to form periodic regular structures, which results in increased energy at the domain boundaries.

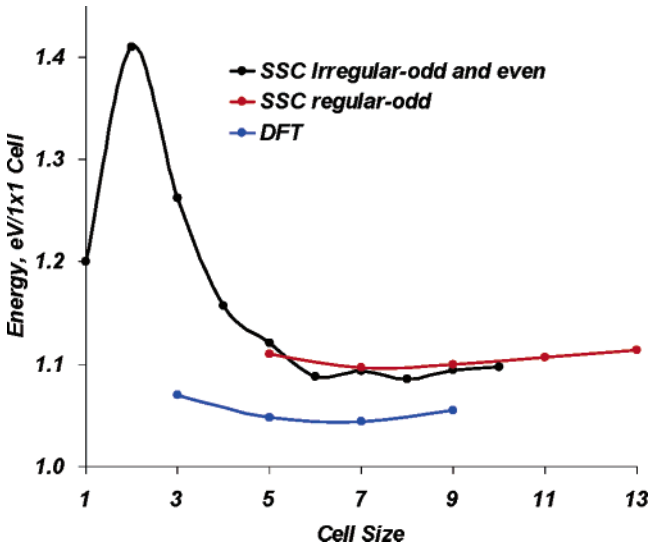

Figure 11. Comparison of DAS and SSC[8] surface energetics. The black dots correspond to the average surface energy of the SSC even-sized and irregular-odd-sized structures in the reconstructed region. The red dots provide the corresponding values for the regular-odd-sized structures (which yield DAS structures), and the blue dots indicate the DFT surface energies of the DAS models. These results show that the normalized SSC energy in the reconstructed region follows a trend similar to the DFT−DAS surface energy, explaining the origin of a finite cell size in the optimum reconstruction.

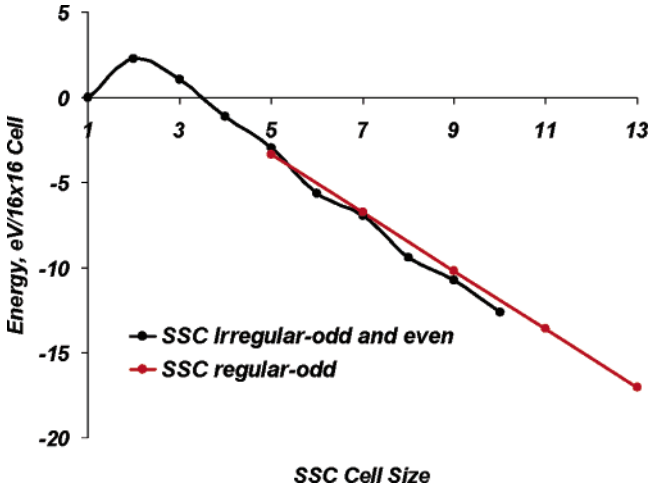

Figure 12. Calculated total surface energy for a 16 × 16 surface cell of Si(111) undergoing the structure changes described by the SSC model of Shimada and Tochihara.[8] These calculations do not account for the energy cost of bringing additional atoms into the system, but this is consistent with the atom type energy contributions presented in Table 6, which depend only on the number of features observed in the surface structure. The monotonic behavior of this graph suggests that the cell size of the reconstructed region should increase indefinitely because the energy seems to decrease indefinitely, but considering the normalized surface energy of the reconstructed region leads to a different conclusion (Figure 11).

(Note that the energy curves in Figure 11 consider only the *average* surface energy in the reconstructed domain but do not take into account what happens outside that domain or whether periodic structures are feasible for each particular structure.) The higher SSC energy with respect to the ab initio results is also a consequence of the nonperiodicity of the SSC structures and the fact that the area of an isolated reconstructed region in the SSC model is larger than the corresponding *n* × *n* cell, thus leading to a less optimal proportion of surface features.

Figure 12 shows the total energy of the 16 × 16 supercell used in the analysis (relative to the initial unreconstructed structure) for the different SSC stages.[8] Except for $n = 2$, the total energy decreases monotonically as the size of the reconstructed domain increases. The graph also indicates that the decrease in energy is greater when the reconstructed domain size increases from an odd size to an even size. This monotonic behavior of the total energy suggests that the size of the reconstructed region should increase indefinitely, but the results of Figure 11 show that the greatest *normalized* gain in stability is obtained for a cell size of 7 × 7, thus explaining the origin of a finite cell size.

These results support the experimental conclusions of Shimada and Tochihara[8] that the formation of the faulted half of the unit cell is the key process in the Si(111) surface reconstruction and the experimental observations that the greatest gain in stability is achieved with the DAS 7 × 7 structure. The AECM analysis provides additional information on the reconstruction energy path and stability of the different stages of the SSC model, and it identifies the presence of an energy barrier at the 2 × 2 cell size, which suggests that the reconstruction process does not take place at low temperatures.

6. Conclusions and Prospects

We report here consistent PBE DFT calculations for various surface reconstructions of the Si(111) surface, confirming that the DAS 7 × 7 structure has the lowest surface energy, 1.044 eV/1 × 1 cell (1310.12 dyn/cm).

We also develop the atomic energy contribution model (AECM) for decomposing the surface energy into individual contributions of different atom types and apply it to the analysis of a real-time reconstruction process, demonstrating a low-surface-energy pathway leading to the DAS 7 × 7 structure. This confirms that the rate-determining step in the DAS surface reconstruction is the formation of the faulted half of the unit cell, as has been proposed by Shimada and Tochihara[8] on the basis of STM observations. This approach should be useful for studying other reconstruction paths, taking into consideration larger domains or following different stages. In addition, generalizations including adsorbates should be useful for examining the inverse reconstruction process that a DAS 7 × 7 surface undergoes when it is functionalized with hydrogen atoms or methyls. This simple but accurate analysis would also be useful for discrete simulation algorithms such as Monte Carlo and others. We plan next to develop a reactive force field fitted to the ab initio results presented here and apply it to real-time dynamic reconstruction and reaction processes on Si(111) surfaces.

Acknowledgment. This research was partially supported by the Microelectronics Advanced Research Corporation (MARCO) and its Focus Center on Function Engineered NanoArchitectonics (FENA). Sandia is a multiprogram laboratory operated by Sandia Corporation, a Lockheed Martin Company, for the United States Department of Energy's National Nuclear Security Administration under contract DE-AC04-94AL85000. We also acknowledge the contributions of Dr. Adri van Duin in discussions regarding the ReaxFF reactive force field and of Dr. Mario Blanco in compiling the structures and force field files from previous research in our group and in useful discussions throughout the project.

Supporting Information Available: Pseudopotentials and basis sets, slab model calculations, comparison of PBE and LDA surface energies, comparison of PBE DFT Si(111) surface energies to published values from empirical and semi-empirical calculations, spin states, and comparison of 2 × 2 hexagonal and regular surfaces. This material is available free of charge via the Internet at http://pubs.acs.org.

LA052029S